CGU HS Committee on River Ice Processes and the Environment
19th Workshop on the Hydraulics of Ice Covered Rivers
Whitehorse, Yukon, Canada, July 9-12, 2017.

Two-way fluid-structure interaction model of waves propagating in a channel with an ice cover

Ning Liu[1], Jim Kells[2], and Karl-Erich Lindenschmidt[3]
[1]*Global Institute for Water Security, University of Saskatchewan, 11 Innovation Boulevard, Saskatoon, SK, Canada, S7N 3H5;*
Email address: Ning.Liu@usask.ca

[2]*Department of Civil, Geological and Environmental Engineering, University of Saskatchewan, 57 Campus Drive, Saskatoon, SK, Canada, S7N 5A9*
Email address: Jim.Kells@usask.ca

[3]*Global Institute for Water Security, University of Saskatchewan, 11 Innovation Boulevard, Saskatoon, SK, Canada, S7N 3H5*
Email address: Karl-Erich.Lindenschmidt@usask.ca

Rapid flow fluctuations generate waves that may potentially break the ice cover downstream of a hydropower plant. To understand the wave-ice interactions, waves propagating in a channel with an ice cover are studied using a two-dimensional numerical model that loosely couples the fluid-structure interactions (FSI). In the fluid domain, two assumingly incompressible and inviscid fluids exist - air and water. In the solid domain, the ice cover is assumed to be homogenous and elastic. At each time step, a two-way feedback coupling is applied to the model, which solves the hydrodynamics of the fluid flow and the elastic structural behaviour of the ice cover separately, but at the fluid-solid interface, it transfers fluid pressure from the fluid domain to the solid domain and the displacement of the ice cover is transferred back from the solid domain to the fluid domain. Two types of boundary conditions are considered in this paper: (1) the ice cover is fixed at the front and the downstream end; and (2) the ice cover is fixed at the downstream end only. Disturbances are introduced to the fluid domain by generating waves of different properties. The wave-generated bending stress within the ice cover is studied.

1. Introduction

The rapid change of river discharge, a common practice in the hydroelectricity generating industry, is termed hydropeaking. It aims to tailor power generation to consumer demands. Hydropeaking operations can bring about flow fluctuations that are very different from the natural flow regime. Although natural flows exhibit a broad range of variation in quantity and timing on a large temporal scale (e.g. annual) (Allan and Castillo 2007), on a smaller time scale (daily), flow fluctuations induced by hydropeaking can be significantly greater in magnitude and of shorter duration, and the timing can be controlled (Harby and Noack 2013).

The climate of Canada determines that its highest electricity demands occur in the winter months, when rivers are ice covered. In mid-winter, when ice covers remain competent, hydropeaking can fracture the ice cover downstream of the dam. The fractured ice cover becomes unstable and further disturbance by flow fluctuations may result in the mechanical breakup of the cover. Mechanical breakup of a competent ice cover often leads to the destructive consequence of ice jam flooding, which threatens public safety and can damage infrastructure and property assets (Doyle 1988, Wigle et al. 1990, Burrell 2008). One such ice jam event was recorded for the Peace River on 7 January 1982. Abrupt hydropeaking operations occurred at the W.A.C. Bennett Dam when the dam release decreased from 1700 m^3/s to 1000 m^3/s and then increased to 1750 m^3/s within a short time period, leading to ice cover breakup and 9 m thick ice jam about 20 km downstream of Dunvegan (Lindenschmidt et al. 2016). The jam release resulted in a peak flow that raised the water level to 3.4 m higher than the level of the initial ice cover (Lindenschmidt et al. 2015).

The cracks in an ice cover resulting from flow fluctuations are understood to have two stages before the onset of an ice run (Beltaos 2008). In the first stage, when incoming waves arrive, the ice cover undergoes increased water pressure on its bottom until longitudinal fractures are formed along the banks. These fractures are usually termed hinge cracks. Depending on the river width, one or two hinge cracks may form. The mechanism of hinge crack formation is relatively well understood (Daly 1995). It is essentially a static mechanical process that does not involve dynamic forces, which means that fluid dynamics is not needed to solve the problem. The second stage occurs after the formation of hinge cracks. With the excess pressure head being relieved, the middle strip of the ice cover is no longer supported by the riverbanks. A further increase of water level lifts the floating middle ice strip to a higher elevation that it is now free floating. Then the ice strip undergoes mainly two types of stresses: vertical bending due to vertical acceleration of incoming waves and the horizontal bending of the ice cover within a meandering section of a river. Once the bending stresses exceed the cover's flexural strength, the ice cover breaks to form transverse cracks, which reduces the cover into smaller ice chunks. Horizontal bending is generally regarded as the cause of large spaced transverse cracks with distances in the order of 1000 times the ice thickness apart (Beltaos 1990). However, transverse cracks spaced less than 100 meters apart or even less have also been observed in the field, which are believed to be a result of vertical bending (Beltaos 2008).

The mechanisms of vertical bending have been studied analytically and numerically. Based on the theory of beams on an elastic foundation (Hetenyi 1946), Billfalk (1981) developed theoretical explanations for the fracture of an ice cover front. Beltaos (2004) applied the same theory and developed a model without the submergence effect and concluded that the maximum

stresses imposed on the ice cover occur when a quarter of the wavelength advances under the ice cover. Daly (1993, 1995) developed a one-dimensional linearized model to investigate shallow wave propagation in ice covered channels, and found that ice cracking will occur at a wavelength of $2\pi l$ where l is the characteristic length of the ice cover. Shen & Xia (1999) extended Daly's method by including axial forces on the ice cover. Xia & Shen (2002) developed a nonlinear analysis and found that a minimum wave amplitude of 0.2 to 0.8 m is required to crack the ice cover. Nzokou et al. (2011) utilize the finite element method (FEM) to simulate transverse cracking induced by waves. They developed a model called HYDROBEAM that solves the one-dimensional Saint-Venant equations in conjunction with the beam equations on an elastic foundation in a staggered time-step manner. They found that the stresses of waves on an ice cover is dependent on the wavelength so that shorter waves induce the maximum stress to the ice cover when the wave crest is passing along the ice whereas the longer waves induce the highest stress when a quarter of the wavelength advances under the ice cover.

Despite the continuing efforts mentioned above, theoretical challenges in understanding the fracturing mechanisms induced by vertical bending persist and studies capturing the ice displacements and deformations subject to the motion of incoming waves under unsteady situations continue. Firstly, the hydrodynamic forces that an ice cover endures depend on the vertical acceleration at the fluid-solid interface. Therefore, hydrodynamic loads on an ice cover are highly dynamic in nature and must be considered in the transient framework. Secondly, the displacement and the deformation of ice covers should be considered when simulating the flow dynamics, which requires modelling the two-way fluid-structure interaction (FSI).

This study aims to address both challenges by applying a two-way FSI model that interchanges solutions of the fluid and solid domains at each iteration time step. As the convergence of a fully free-floating ice cover in the FSI model is difficult and time-consuming to achieve, at least one end of the ice cover is fixed in this study. Two types of boundary conditions are considered in this paper: (1) the ice cover is fixed at the upstream front and the downstream end; and (2) the ice cover is fixed at the downstream end only. Disturbances are introduced to the fluid domain through generated waves of different properties. The wave-generated bending stress on the ice cover is discussed.

2. Method

2.1 Formulation of the problem

Free-surface flows of an inviscid, incompressible fluid in a flat channel of infinite width and finite depth h that is covered by an elastic ice cover of uniform thickness η, length L, Young's modulus E, and Poisson ratio μ are considered. The fluid moves at velocity U and is irrotational. A small perturbation on the inlet flow velocity $U_{inlet}(t)$ generates waves of relatively small velocity disturbance $\Delta U(t)$ as a function of time t. We introduce Cartesian coordinates x, y, z with the y-axis directed vertically upwards and the x-axis in the direction of the flow. Gravity is acting in the negative y-direction. The displacement of the ice cover is denoted by $y = \xi(x, t)$, where the origin $(0,0,0)$ of the coordinate is defined at the center of mass of the ice cover. The sketch of the system is shown in Figure 1.

This system is simulated using a high-performance computational fluid dynamics (CFD) software tool ANSYS version 18.0 (ANSYS 2017). The model construct is based on ANSYS

CFX's multiphase flow theory and ANSYS Transient Structural analysis. A description of the model design and boundary settings is provided hereafter.

2.2 Model settings

A geometry was created in ANSYS ModelBuilder simulating the model as conceptualized in Figure 1. As CFX only supports 3D models, the domain was built to be of one-mesh-wide in the z-direction to reduce the model to 2D. As illustrated in Figure 2, a solid body of 10 meter in length and 1 m in thickness is resting on the water surface at hydrostatic equilibrium initially, which means that its bottom rests at a height of 4.083m above the channel bottom. This height is determined by its density of 917 kg/m^3 and the density of water that it floats on, which is 1000 kg/m^3. The solid body has Young's modulus of 6.5 GPa and a Poisson ratio of 0.35. The fluid domain is set to be 10 m in height and 100 m in length. The water level is set to be 5 m when no disturbance occurs, with the above air having a density of 1.185 kg/m^3. The free surface between the air and the water is controlled by ANSYS CFX's multiphase flow solver.

Figure 3 demonstrates the setting of the domains. In the fluid domain (Figure 3a), water flows into the domain from the left boundary at a rate governed by the function U(t). Both the upper left and right boundaries are set to be openings so that water will flow out from the right and air is free to flow in and out of the domain from both sides. The upper boundary is set to be an opening too. Atmospheric pressure is set to be 1 atm at all opening boundaries. The boundaries at the front and back faces are set to be symmetrical, which complies with the assumption of an infinitely wide channel described in the problem formulation section. The boundary at the bottom of the domain is a non-slip wall. In the solid domain, the boundary conditions are set as either the upstream front and downstream end of the ice cover being fixed for boundary condition 1 (BC1, Figure 3b) or only the downstream end of the ice cover being fixed (BC2, Figure 3c). The upper, bottom and front surfaces of ice are set to be the fluid-solid interfaces, where the coupling feedbacks are interchanged.

The flow dynamics is governed by the conservation of mass, momentum and energy. Because thermal effects are not considered in this model, energy conservation is ignored. The forces generated in the fluid domain on the fluid-solid interfaces are transferred at each iteration timestep to the solid domain, where deformation and displacement of the solid body is calculated and the motion in the y-direction y is then transferred back to the fluid domain. The water free surface is simulated in ANSYS CFX using the volume of fraction (VOF) equations based on volume percentage of air and water at each mesh.

2.3 Numerical solution procedure

ANSYS CFX uses an element-based finite volume method. All solution variables and fluid properties are stored at the nodes (mesh vertices). A high resolution scheme is selected for the spatial discretization, while second order backward Euler scheme (SOBE) is applied to discretize time. The SOBE scheme is an implicit time-stepping scheme, and is of second-order accuracy.

The convergence criteria were set to be $< 10^{-4}$ of the root mean square of the residuals for both conservation of mass and momentum in both x- and y- directions. The simulation domain was discretized to hexahedral and tetrahedral mesh elements in the fluid and the solid domains. Mesh independence tests and time step sensitivity tests were carried out to eliminate inaccuracies

induced by discretization errors, indicating that mesh sizes < 0.4 m and a time step interval = 0.025 s provide optimum results.

2.4 Scenario settings and data analysis methods

Although it is recognized that the negative consequences can be induced by hydropeaking operations, studies that quantify the impact of these rapid fluctuations on ice covers are rare. The tool developed by Sauterleute and Charmasson (2014) analyzed the times series of flow and stage data in five Norwegian rivers. However, the time series available by gauging stations were normally on a time scale larger than one hour, which will omit waves with relatively high frequency. Munk (1950) classifies surface waves into seven categories, the "ordinary gravity waves" category being the most common that "can be noticed with the naked eye" (Munk 1950), with periods ranging from 1 to 30 seconds (i.e. frequency between 0.033 and 1 s^{-1}). Although the classification was originally used in ocean engineering, it can be transferred to freshwater gravity waves because both are driven by gravity as the restoring force. It is reasonable that the spectrum of hydropeaking waves shall fall into the ordinary gravity wave category assuming uniform flat channel and inviscid and incompressible water properties.

A user defined inlet equation was set up to generate scenarios capturing various incident wave conditions as in [1]:

$$U(t) = U_{x0} + U_{xd} \cdot \sin[2\pi \cdot f \cdot min(t - t_{on,}\, D)] \quad [1]$$

where U_{x0} is the initial velocity in the *x*-direction, U_{xd} is the maximum value of velocity disturbances in the *x*-direction, f is the frequency of rise and fall of the disturbances, t and t_{on} are the current time and the time that the disturbances start, and D is the duration of the disturbances. The waves are sinusoidal but are of various magnitude, frequency, and duration of disturbances. The inlet equation generates waves with the desired property by fluctuating the values of velocity. Table 1 summarizes the scenarios set in the simulations. All scenarios were carried out for the two types of boundary conditions in a 2-D channel as summarized in Table 1. The transient results at each time step are exported using ANSYS CFD-Post by a user-defined command file. The data contain coordinates and pressure at each node of the solid body. For each scenario, the pressure distribution along the length of the ice cover evolving over time was analyzed. Analyses were conducted using Python 3.5 with the Numpy, Pandas, and Matplotlib packages.

3. Results and discussions

Before running each scenario, the simulations were pre-run at constant settings for 10 seconds to stabilize the coupling of fluid and solid interactions. Boundary condition 1 (BC1) denotes the case that ice cover is fixed at both the upstream and downstream ends, whereas Boundary condition 2 (BC2) only fixes the downstream end. Following the scenarios set in Table 1, disturbances were introduced after 10 seconds and simulations were run for 30 seconds. Pressure profiles on each mesh of the ice bottom at each time step were extracted and plotted. The hydrostatic pressure of ice of 1 m thick is equal to 8995 Pa (i.e. $\rho_{water} \cdot g \cdot h_{submerged} = 1000\ kg/m^3 \times 9.81 m/s^2 \times 0.917 m$). Results of the scenarios of each situation are compared below.

3.1 Effects of inlet velocity

Figure 4 demonstrates the evolving of pressure with time induced by water waves on ice cover bottom, in which the magnitude (0.2 m/s), frequency (0.2 s^{-1}), and duration (20 s) of the disturbances were kept constant but the inlet velocity was different. In BC1 (i.e. Figure 4a, 4b, 4c, and 4d, water pressure displays a similar pattern as that using the BC2 (i.e. Figure 4e, 4f, 4g and 4h). In both types of boundary conditions, hydraulic pressure obtains larger peaks when inlet flow is smaller, but larger troughs when the flow is larger. In other words, when inlet flow is smaller, pressure larger than the hydrostatic pressure prevails; on the contrary, pressure smaller than hydrostatic pressure prevails at faster inlet flow scenarios. Comparing to BC1, in BC2, the free displacement of the upstream front of the ice cover appears to delay the occurrence of pressure peaks.

3.2 Effects of disturbance magnitude

Figure 5 demonstrates the pressure distribution evolving with time as the waves move along the ice cover bottom, in which the frequency (0.2 s^{-1}), and duration (20 s) of the disturbances, as well as the inlet velocity (0.5 m/s) were kept constant but the disturbance magnitude differs. For BC1 (i.e. Figure 5a, 5b, 5c and 5d, water pressure displays similar patterns as those for BC2 (i.e. Figure 5e, 5f, 5g and 5h). In both types of boundary conditions, the pressure profiles demonstrate higher fluctuation intensity when the disturbance magnitudes are larger. Again, freeing the motion of the upstream front of the ice cover delayed the time that the disturbance obtains its peak value.

3.3 Effects of disturbance frequency

Figure 6 demonstrates the changing of pressure profile with time as the waves travelling along the ice cover, in which the magnitude (0.2 m/s) and duration (20 s) of the disturbances as well as the inlet velocity (0.5 m/s) were kept constant but the disturbance frequency varies. Results of BC1 are presented in Figure 6a, 6b, 6c and 6d, whereas the results for BC2 are shown in Figure 6e, 6f, 6g and 6h. High frequency waves dissipate their energy faster than those of low frequencies, hence the pressure fluctuations appear minimal in Figure 6d and 6h. However, the discretization scheme adopted in this study could also lead to different dissipations for variable changes at different frequency. The quantification of numerical dissipation is to be investigated in future work. It can also be observed in Figure 6 that the onset of pressure fluctuations is different in BC1 and BC2. At a different fluctuation frequency, either delay or advancement of the onset time step of the pressure peak can be expected in BC2. The frequency of pressure fluctuations appears to comply with that of the incoming disturbances in both types of boundary conditions.

4. Conclusion

The transient interactions between an ice cover and incoming waves were studied for a channel with one or two edges in the longitudinal direction being fixed. The ice cover is assumed to be homogenous and elastic. Fluids in the simulations are both inviscid and incompressible. It is found that allowing the ice cover to displace at one end will modify the resulting pressure field induced by the flow on the ice bottom. However, the displacement of an ice cover does not modify the frequency of ordinary gravity waves passing by. Further study is need to explore the extent of numerical dissipations and the effect of freeing both edges on the pressure distributions.

Acknowledgments
Financial support for this work was provided through NSERC Discovery and Engage grants, Saskatchewan Innovation & Opportunity Scholarship, and the Canada Excellence Research Chair at the Global Institute for Water Security (GIWS), which is gratefully acknowledged.

References

Allan, J.D. and Castillo, M.M., 2007. Stream ecology: Structure and function of running waters. 2nd Ed. Springer.

ANSYS Inc. (2017). ANSYS CFX-Solver Theory Guide, Release 18.0. Retrieved from online documentation, www.ansys.com.

Beltaos, S. (1990). Fracture and breakup of river ice cover. Canadian Journal of Civil Engineering, 17(2), 173-183.

Beltaos, S. (2004). Wave-generated fractures in river ice covers. Cold Regions Science and Technology, 40(3), 179-191.

Beltaos, S., (Ed.). (2008). River ice breakup, Water Resources Publications, Highlands Ranch, CO.

Burrell, B. C., 2008. Introduction. River ice Breakup, S. Beltaos, ed., Water Resources Publications, Highlands Ranch, Co.

Daly, S. F. (1993). Wave propagation in ice-covered channels. Journal of Hydraulic Engineering, ASCE, 119(8), 895-910.

Daly, S.F. (1995). Fracture of river ice covers by river waves. Journal of Cold Regions Engineering, ASCE, 9(1), 41-52.

Doyle, P. F. (1988). Damage resulting from a sudden river ice breakup, Canadian Journal of Civil Engineering, 15, 609-615.

Harby, A., and Noack, M., 2013. Rapid Flow Fluctuations and Impacts on Fish and the Aquatic Ecosystem. Ecohydraulics: An Integrated Approach, 323-335.

Hetényi, M. (1946). Beams on Elastic Foundation. Theory with Applications in the Fields of Civil and Mechanical Engineering. The University of Michigan Press, Ann Arbor.

Lindenschmidt, K. E., Das, A., Rokaya, P., Chun, K., and Chu, T. (2015). Ice jam flood hazard assessment and mapping of the Peace River at the Town of Peace River. CGU HS Committee on River Ice Processes and the Environment, 18th Workshop on the Hydraulics of Ice Covered Rivers. Quebec City, QC, Canada, August 18-20, 2015.

Lindenschmidt, K. E., Das, A., Rokaya, P., and Chu, T. (2016). Ice jam flood risk assessment and mapping. Hydrological Processes, 30(21), 3754-3769.

Munk, W. H. (1950). Origin and generation of waves. Proceedings 1st International Conference on Coastal Engineering, ASCE, Long Beach, California (1950), pp. 1–4. Nzokou, T. F., Morse, B., Robert, J-L., Richard, M., and Tossou, E. (2011). Water wave transients in an ice-covered channel. Canadian Journal of Civil Engineering. 38(4), 404-414.

Nzokou, F., Morse, B., Robert, J-L., Richard, M., and Tossou, E. (2011). Water wave transients in an ice-covered channel. Canadian Journal of Civil Engineering. 38(4), 404-414.

Sauterleute, J. F., and Charmasson, J. (2014). A computational tool for the characterisation of rapid fluctuations in flow and stage in rivers caused by hydropeaking. Environmental Modelling & Software, 55, 266-278.

Shen, H.T. and Xia, X., 1999. Nonlinear interaction of surge waves with ice cover in river channels (No. 375-661). Department of Civil and Environmental Engineering, Clarkson Univeristy Potsdam New York.

Wigle, T., Doyle, P., Fonsera, F., Mark, H., Parmley, L., Raban, R, and Roberts, S. (1990). Optimum operation of hydroelectric plants during the ice regime of rivers – A Canadian experience. Prepared by a Task Force of the Subcommittee on Hydraulics of Ice-Covered Rivers, National Research Council of Canada, Ottawa.

Xia, X., and Shen, H. T. (2002). Nonlinear interaction of ice cover with shallow water waves in channels. Journal of Fluid Mechanics, 467, 259-268.

Figures and Tables:

Table 1. Scenario settings

Tests on:	Inlet velocity m/s	Disturbance magnitude m/s	Frequency s^{-1}	Duration s
Inlet velocity	0.3	0.2	0.2	20
	0.5	0.2	0.2	20
	0.8	0.2	0.2	20
	1.0	0.2	0.2	20
Fluctuation	0.5	0.04	0.2	20
	0.5	0.08	0.2	20
	0.5	0.2	0.2	20
	0.5	0.4	0.2	20
Frequency	0.5	0.2	0.05	20
	0.5	0.2	0.1	20
	0.5	0.2	0.2	20
	0.5	0.2	0.5	20

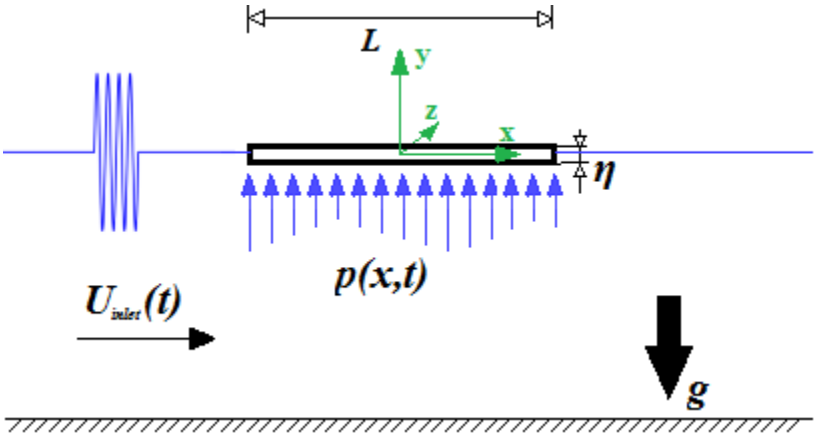

Figure 1. Sketch of the model

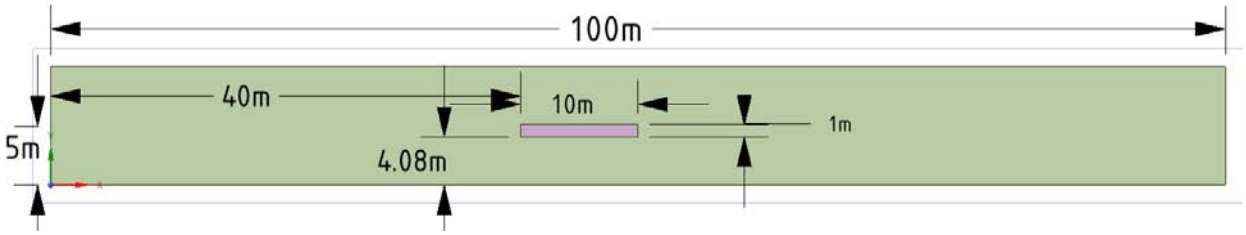

Figure 2. Dimensions of the model

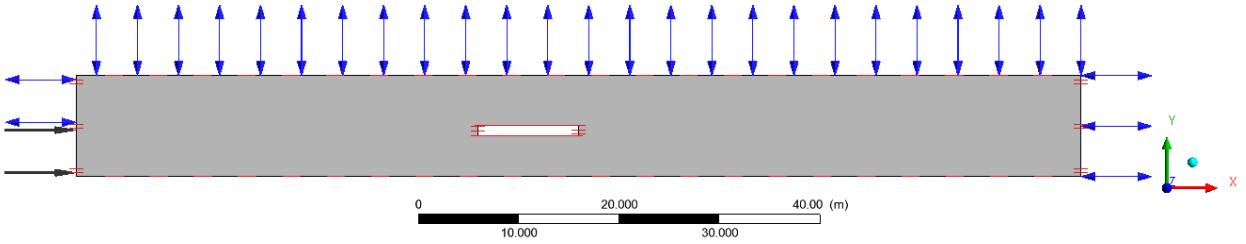

(a)

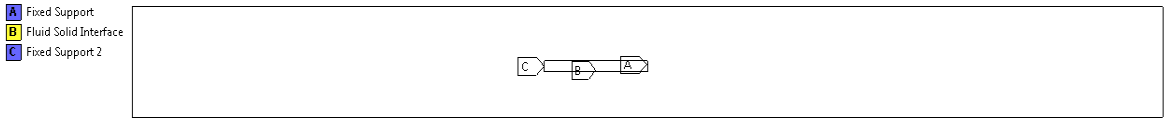

(b)

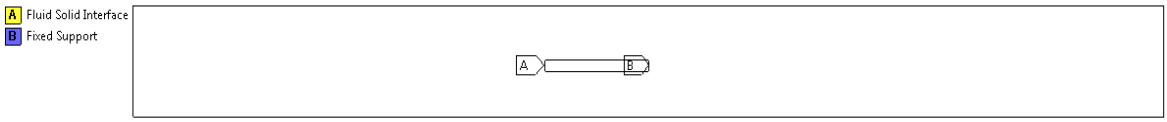

(c)

Figure 3. Boundary settings of the fluid and the solid domains

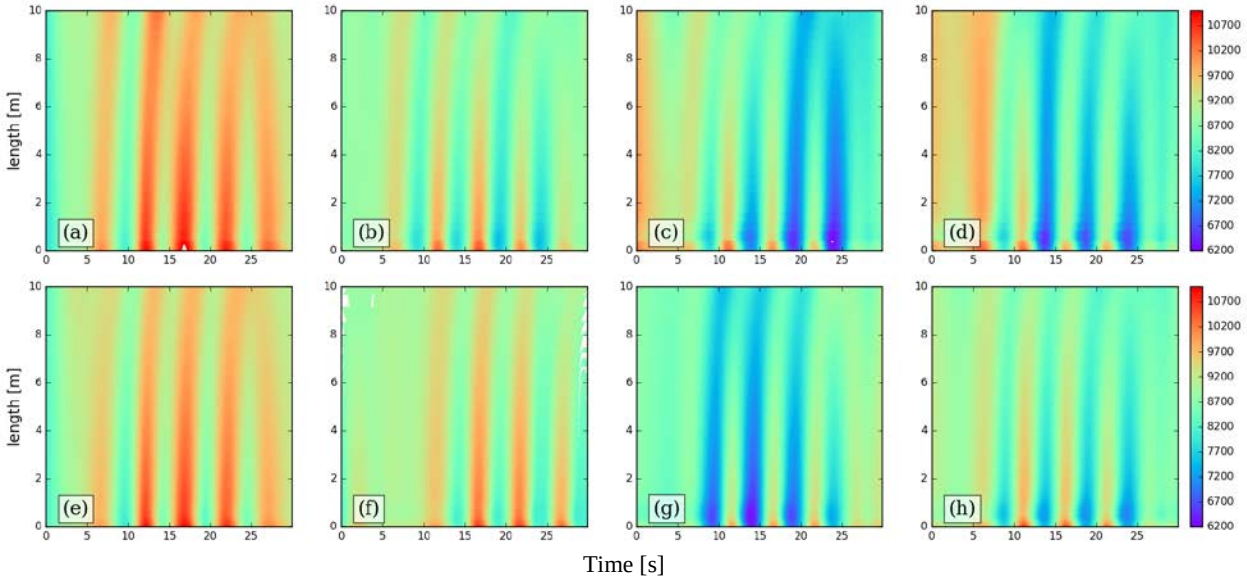

Figure 4. Evolving of hydraulic loads with time on the bottom of ice cover with disturbances at different inlet velocity. BC1 is indicated by the figures on top and BC2 on bottom: from left to right, inlet velocity $\boldsymbol{U_{x0}}$ is 0.3 m/s, 0.5 m/s, 0.8 m/s, and 1 m/s. The color bars on the right denote pressure magnitude in Pa.

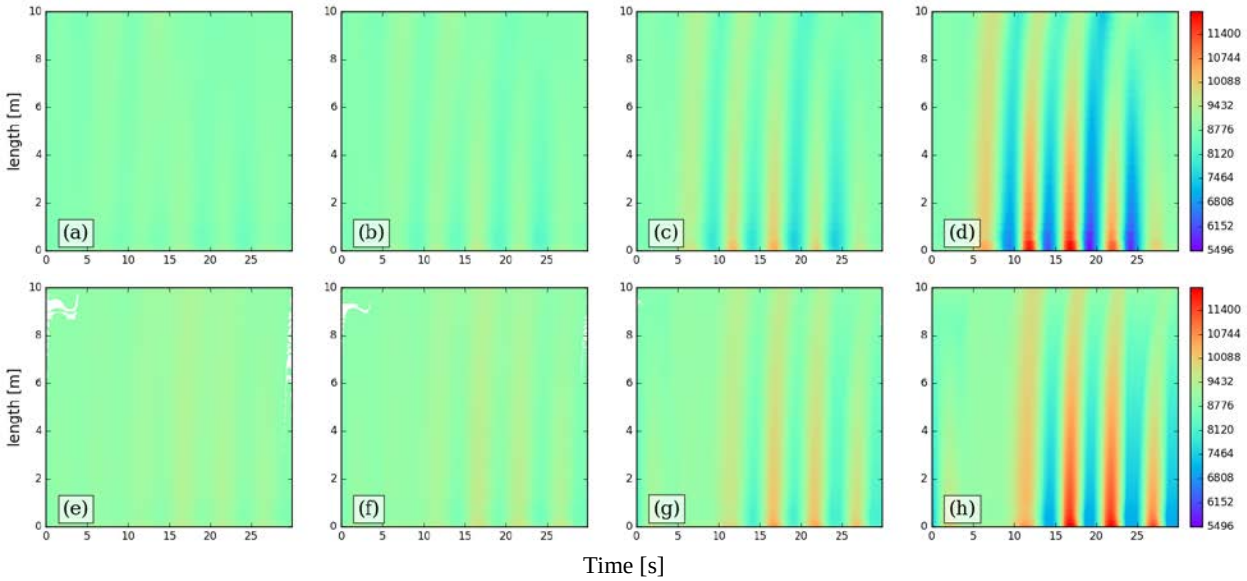

Figure 5. Evolving of hydraulic loads with time on the bottom of ice cover with disturbances at different velocity magnitude. BC1 is indicated by the figures on top and BC2 on bottom: from left to right, inlet velocity $\boldsymbol{U_{xd}}$ is 0.04 m/s, 0.08 m/s, 0.2 m/s, and 0.4 m/s. The color bars on the right denote pressure magnitude in Pa.

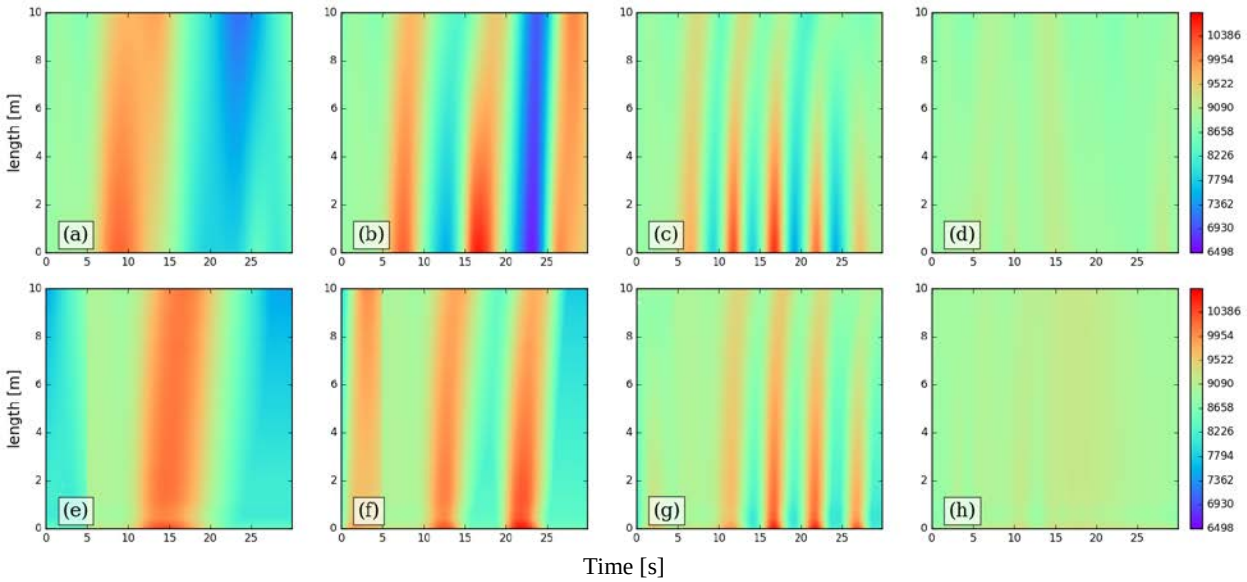

Figure 6. Evolving of hydraulic loads with time on the bottom of ice cover with disturbances of different frequency. BC1 is indicated by the figures on top and BC2 on bottom: from left to right, inlet velocity $\boldsymbol{f}$ is 0.05 s^{-1}, 0.1 s^{-1}, 0.2 s^{-1}, 0.5 s^{-1}. The color bars on the right denote pressure magnitude in Pa.